

Development of a full-scale magnetorheological damper model for open-loop cable vibration control

Ru Zhang^{1,2}, Yi-Qing Ni³, Yuanfeng Duan^{*2} and Jan-Ming Ko³

¹Department of Civil Engineering, Zhejiang University City College, Hangzhou 310015, P. R. China

²College of Civil Engineering and Architecture, Zhejiang University, Hangzhou 310058, P. R. China

³Department of Civil and Environmental Engineering, The Hong Kong Polytechnic University, Kowloon, Hong Kong, P. R. China

(Received September 25, 2018, Revised December 20, 2018, Accepted January 17, 2019)

Abstract. Modeling of magnetorheological (MR) dampers for cable vibration control to facilitate the design of even more effective and economical systems is still a challenging task. In this study, a parameter-adaptive three-element model is first established for a full-scale MR damper based on laboratory tests. The parameters of the model are represented by a set of empirical formulae in terms of displacement amplitude, voltage input, and excitation frequency. The model is then incorporated into the governing equation of cable-damper system for investigation of open-loop vibration control of stay cables in a cable-stayed bridge. The concept of optimal voltage/current input achieving the maximum damping for the system is put forward and verified. Multi-mode suboptimal and Single-mode optimal open-loop control method is then developed. Important conclusions are drawn on application issues and unique characteristics of open-loop cable vibration control using MR dampers.

Keywords: magnetorheological (MR) damper; vibration control; stay cable; open-loop control

1. Introduction

Vibration control of stay cables has received considerable attention during the last decades (Virlogeux 1998, Johnson *et al.* 2007, Zhou *et al.* 2014, Sun *et al.* 2017, Wang *et al.* 2005, Wang *et al.* 2018, Zhou *et al.* 2018). The cables of the cable-stayed bridges are prone to vibrations with excessive or unanticipated amplitudes by external excitations (e.g., wind, rain, support motion), owing to their low intrinsic damping and high flexibility (Hikami and Shiraishi 1988, Ko *et al.* 2002, Chen *et al.* 2004, Jing *et al.* 2016). Magnetorheological (MR) dampers have been proposed for the cable vibration mitigation by various experimental and analytical studies, and engineering applications as well (Carlson and Spencer 1996, Ko, *et al.* 2003, Duan 2004, Duan *et al.* 2005, 2006, 2009a, b, Jung *et al.* 2004, Li *et al.* 2007, Guan *et al.* 2012, Huang *et al.* 2015, Wang *et al.* 2019). The smart MR damping system for cable vibration control has salient advantages over passive or fully active control systems, in either open-loop control mode or closed-loop control mode (Hikami and Shiraishi 1988, Pacheco and Fujino 1993, Matsumoto *et al.* 1995, Poston 1998, Verwiebe 1998, Persoon and Noorlander 1999, Tanaka 2003, Ni *et al.* 2007). In the open-loop control mode, MR dampers of same size can be used for cables of different configurations in a cable-stayed bridge to achieve optimal or suboptimal control effectiveness; through altering the input of voltage/current to the dampers, the MR dampers can achieve optimal or

suboptimal control effectiveness for different modes under different vibration amplitudes that cannot be specified a priori. In the closed-loop control mode, with the aid of an appropriate control strategy, the semi-active MR dampers can achieve much better damping effectiveness than optimal passive dampers, but at much less cost or with lower power requirements than fully active control systems.

Due to the intrinsic nonlinearity and changeable damping nature of MR dampers, development of control strategies that are practically implementable and can fully utilize the semi-active capability of MR dampers and modeling of MR dampers to facilitate the implementation of control strategies is still a challenging task. On one hand, the control strategies should take into account the characteristics of both the hosting structures – stay cables and the damping devices – MR dampers. On the other hand, although a number of mathematical models for MR dampers are available (Butz and Stryk 2002, Jung *et al.* 2004, Kazakov *et al.* 2016), very few are convenient for structural control design. In control design, the model of MR dampers has to be integrated with the governing equation of the controlled structure hosting the dampers. Therefore, a simple, yet reasonably accurate model, which relies on a limited number of parameters and therefore can be easily incorporated into the control strategies, is desired. In order to facilitate the damper design in engineering implementation, a general formula has been proposed (Duan 2004, Duan *et al.* 2006) that evaluates the achieved damping ratio of the cable-damper system, taking into account damper mass, damper stiffness, stiffness of damper support, nonlinearity of damper, as well as the cable sag and inclination. Based on this general formula, the design of open-loop control strategies for single-mode optimal control and multi-mode suboptimal control becomes direct and

*Corresponding author, Professor
E-mail: ceyfduan@zju.edu.cn

convenient in an analytical way. In the derivation of this general formula, the damper was modeled as a mechanical analogue consisting of a viscous dashpot, a spring, and a frictional element in parallel - the three-element model originally proposed for electrorheology (ER) dampers by Powell (1994). The coefficients of these three elements were regarded as changeable with input voltage/current, vibration frequency and amplitude. However, the relationship between these parameters with the voltage/current inputs for MR dampers under different operation conditions (with different vibration amplitudes and frequencies) and how to incorporate the model into control strategies for practical application remain unaddressed. In this paper, we address these two issues by exploring the modeling of a full-scale MR damper and demonstrating its application in vibration control design of a typical stay cable on a cable-stayed Bridge.

Laboratory tests are first carried out by means of sinusoidal excitation with different frequencies, amplitudes, and voltage/current inputs to the MR damper. The hysteresis loops of force versus displacement, and force versus velocity are obtained. Then the parameters of the three-element model are identified from the experimental data and expressed by polynomial functions in terms of vibration frequency, amplitude, and voltage input. Thus a parameter-adaptive three-element model is fully developed. By incorporating the damper model into the general formula, the open-loop control strategies can be directly implementable by altering the voltage/current inputs to the dampers, taking into account damper mass, damper stiffness, stiffness of damper support, nonlinearity of damper, and inclination and sag of the cable. The control strategies and implementation issues are addressed.

2. Test description and results

A linear stroke damper RD-1005 (Fig. 1) manufactured by Lord Corporation was adopted in the tests. The damper is 15.5 cm long in its extended position, and has a stroke of ± 2.5 cm. The main cylinder is 3.8 cm in diameter and houses a piston, a magnetic circuit, an accumulator, and 50 ml of MR fluid. The MR fluid valve is formed by an annular orifice and an associated magnetic circuit that is fully contained within the piston. A controllable force of the range of 50-2500 N can be generated by this damper. The force is stable over a broad temperature range, varying by less than 10% in the range of $-40 - 150^{\circ}\text{C}$. The resistance of the magnetic circuit is about 5 Ohms at an ambient temperature of 25°C , and the maximum voltage/current input is 10V/2A (Carlson and Spencer 1996). Although the damper contains approximately 50 ml of MR fluid, the actual amount of fluid that is activated in the magnetic valve at any given instant is only about 0.3 ml. It is interesting to note that an ER fluid damper of comparable performance would require about 30 ml of active fluid in the valve at any given instant (Carlson and Spencer 1996).

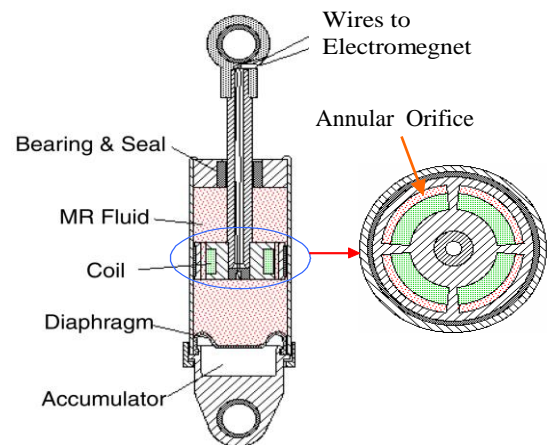


Fig. 1 MR damper RD-1005 (Lord Corporation)

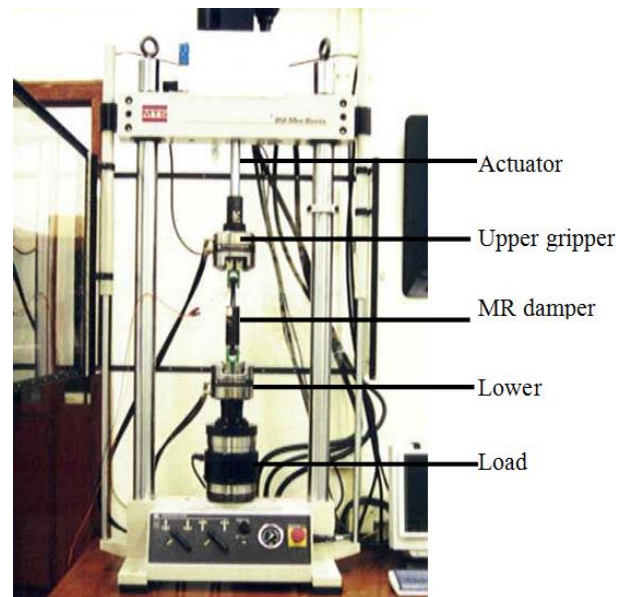
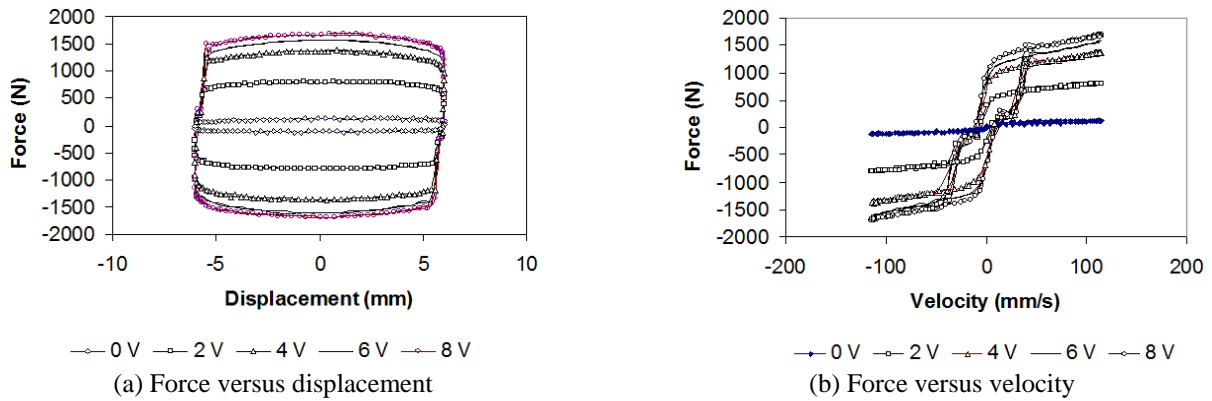
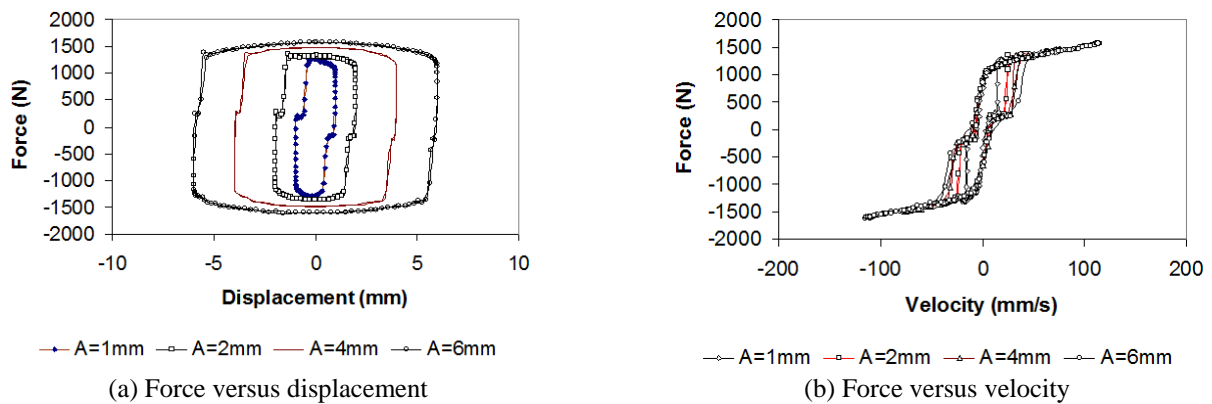
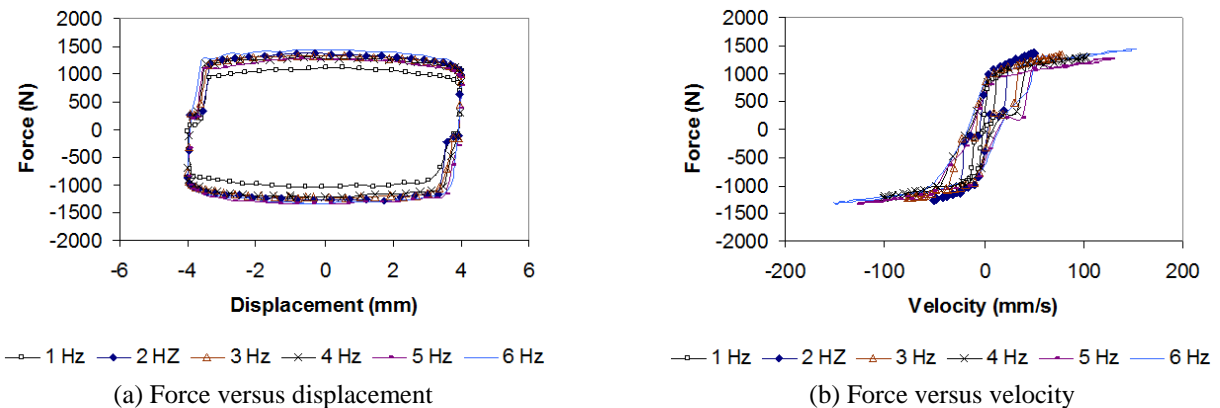


Fig. 2 Experimental setup

As shown in Fig. 2, the MR damper was tested in a computer-controlled MTS machine (Model 858, 15 kN). The MR damper is installed between the upper and lower grippers. The upper moving arm is actuated through the computer-controlled hydraulic supplier, while the lower arm is fixed. The load cell is located in the lower static arm; therefore, its acceleration equals zero and the measured force is the exact force exerted on the rod of the damper.

Tests of sinusoidal vibration were carried out at frequencies of 1 Hz to 6 Hz, displacement amplitudes of 2 mm to 8 mm, and voltage inputs of 0 V to 8 V. Typical results are shown in Figs. 3-5, with hysteresis loops of force versus displacement and force versus velocity. The results represent three categories of tests: (i) To investigate the variation of hysteresis loops with voltage input V at a given

Fig. 3 Experimental hysteresis loops with different voltage inputs ($f = 3$ Hz, $A = 6$ mm)Fig. 4 Experimental hysteresis loops with different amplitudes ($f = 3$ Hz, $V = 6$ V)Fig. 5 Experimental hysteresis loops with different frequencies ($A = 4$ mm, $V = 4$ V)

frequency f and amplitude A . Fig. 3 shows the results of $f = 3$ Hz and $A = 6$ mm, with the voltage input V varying from 0 V to 8 V. The damper force is found to increase as the voltage input increases, but the rate of increase gradually decreases due to magnetic saturation. (ii) To investigate the variation of hysteresis loops with vibration amplitude A at a given frequency f and voltage input V . Fig. 4 shows the results of $f = 3$ Hz and $V = 6$ V, with a displacement amplitude A of 1 mm, 2 mm, 4 mm, and 6 mm. It is clear that for the given excitation frequency and voltage input,

the damper force shows a slight but evident increase as the displacement amplitude increases. (iii) To investigate the variation of hysteresis loops varying with excitation frequency f at a given amplitude A and voltage input V . Fig. 5 shows the results of $A = 4$ mm and $V = 4$ V, with the frequency varying from 1 Hz to 6 Hz. It is observed that both the force-displacement and force-velocity hysteresis loops are dependent on the frequency. Therefore, when modelling the damper it is necessary to consider the effect of the frequency, as well as the voltage input and the vibration amplitude.

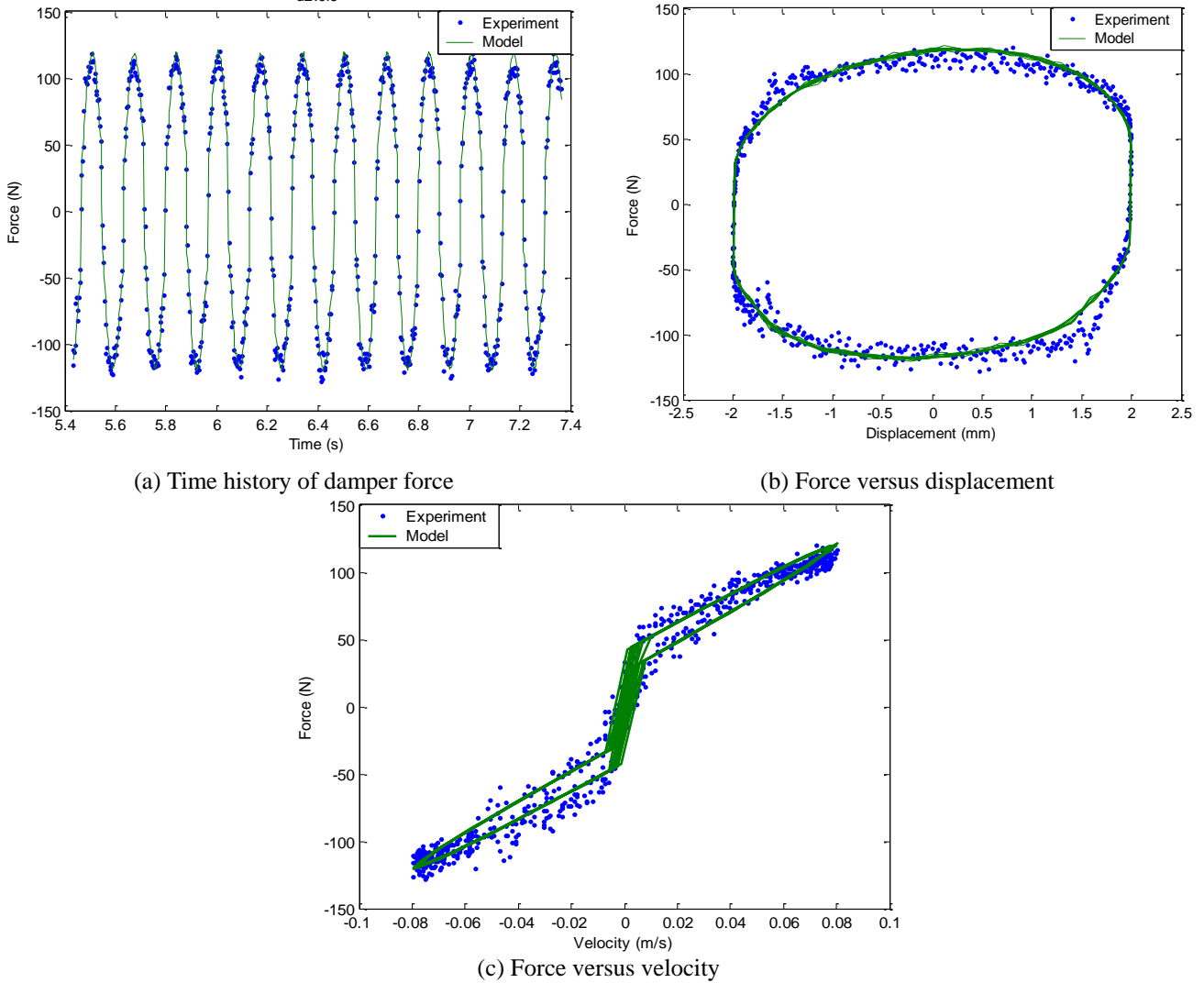


Fig. 6 Comparison of the model with the experimental data ($A = 2 \text{ mm}$, $V = 0 \text{ V}$, $f = 6 \text{ Hz}$)

3. Proposed model and parameter identification

Due to its simplicity in expression and satisfactory accuracy in representing the characteristics of MR dampers, the well-known three-element model (Powell 1994) is adopted here. In the mechanical analogue of the three-element model, if k_e is the stiffness coefficient, c_e is the viscous coefficient, and F_l is the frictional coefficient, the damper force can be expressed as

$$F = k_e x + c_e \dot{x} + F_l \text{sign}(\dot{x}) \quad (1)$$

It should be noted that the three parameters k_e , c_e , and F_l are dependent on the vibration frequency, displacement amplitude, and voltage/current input, as will be discussed in detail later.

By using the nonlinear least-square method, the three parameters can be identified from the experimental data by minimizing the error of

$$\text{Error}_F = \sum \left| F_i - k_e x_{t_i} + c_e \dot{x}_{t_i} + F_l \text{sign}(\dot{x}_{t_i}) \right|^2 \quad (2)$$

where t_i is the sampling instant during the experiments.

Figs. 6 and 7 show two cases of the identified model compared with the experimental data. In the former case, the displacement amplitude $A = 2 \text{ mm}$, the voltage input $V = 0 \text{ V}$, and the vibration frequency $f = 6 \text{ Hz}$; while in the latter case the displacement amplitude $A = 6 \text{ mm}$, the voltage input $V = 6 \text{ V}$, and the vibration frequency $f = 1 \text{ Hz}$. The two cases show that the proposed model can well represent the hysteresis loops of force versus displacement and force versus velocity, as well as the time history of the damper force.

The identified parameters, k_e , c_e , and F_l , are dependent on the voltage/current input, displacement amplitude, and vibration frequency. A set of empirical formulae have been obtained through curve fitting to characterize the dependence. Figs. 8-10 show the dependence of the stiffness coefficient k_e .

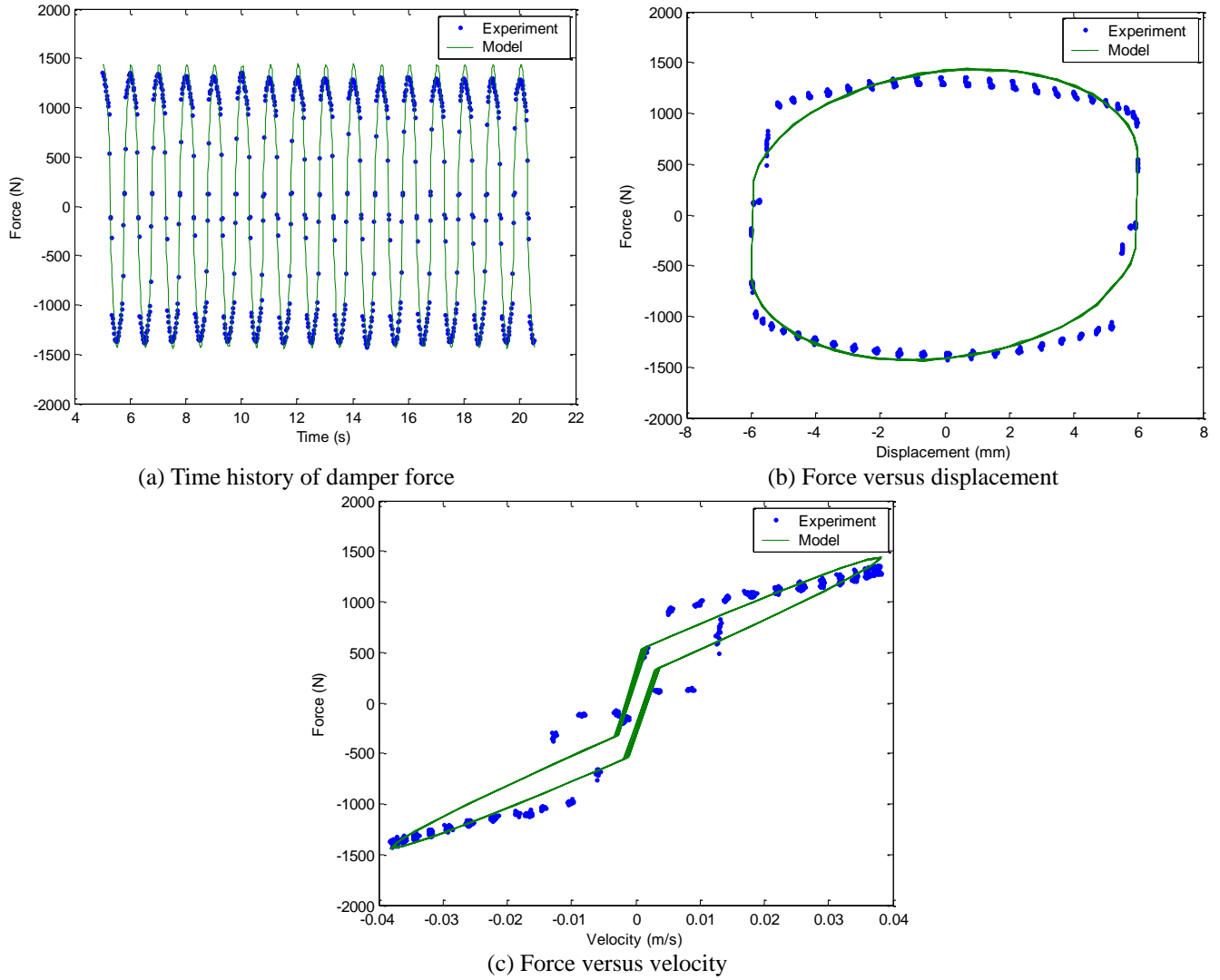


Fig. 7 Comparison of the model with the experimental data ($A = 6$ mm, $V = 6$ V, $f = 1$ Hz)

The circles represent the identified values of the parameter from the experimental data, while the dashed line shows the results of empirical formulae that will be discussed later. It is found that the dependence of the stiffness coefficient k_e on voltage input V , displacement amplitude A , and vibration frequency f can be expressed by a second-order polynomial of the three parameters, respectively. Figs. 11-13 show the dependence of the viscous coefficient c_e . It turns out that the viscous coefficient c_e is of the second order of polynomial of the voltage input V and the vibration frequency f , but is proportional to the displacement amplitude A . Similarly, it is seen from Figs. 14-16 that the frictional coefficient F_l is also of the second order of polynomial of the voltage input V and the vibration frequency f , but is proportional to the displacement amplitude A . Therefore, through nonlinear least square method, the empirical formulae of the stiffness coefficient k_e , the viscous coefficient c_e , and the frictional coefficient F_l can be given as

$$k_e = (2.780A^2 - 32.457A + 103.644) \cdot (-18.689V^2 + 330.274V + 22.299) \cdot (-0.560f^2 + 2.934f - 0.409) + 516.992 \quad (3a)$$

$$c_e = 1000(-1.560A + 12.867) \cdot (-0.099V^2 + 1.573V + 0.320) \cdot (0.065f^2 - 0.572f + 1.590) - 367.734 \quad (3b)$$

$$F_l = (1.801A + 1.476) \cdot (-0.919V^2 + 12.009V + 1.987) \cdot (-0.188f^2 + 0.999f - 0.088) + 34.486 \quad (3c)$$

The empirical formulae (marked by dashed lines) fit well with the experimental results (marked by circles) as illustrated in Figs. 8-16. The relative errors of these empirical formulae are within 10% for a displacement amplitude $A = 0 - 7$ mm, a voltage input $V = 0 - 6$ volts, and a vibration frequency $f = 0 - 5$ Hz, which is a broad enough range for the actual application in the open-loop control of rain-wind-induced cable vibration.

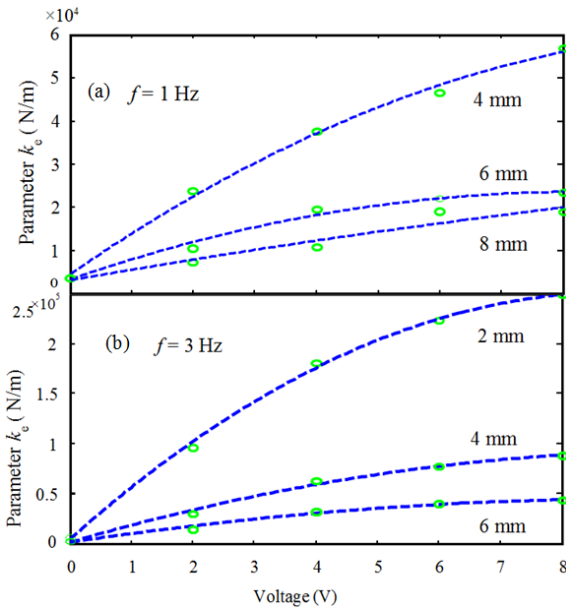


Fig. 8 Dependence of the stiffness coefficient k_e on the voltage input V

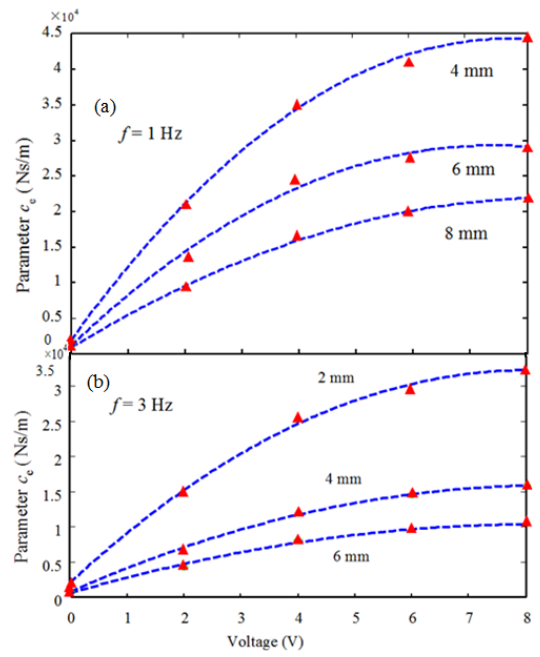


Fig. 11 Dependence of the viscous coefficient c_e on the voltage input V

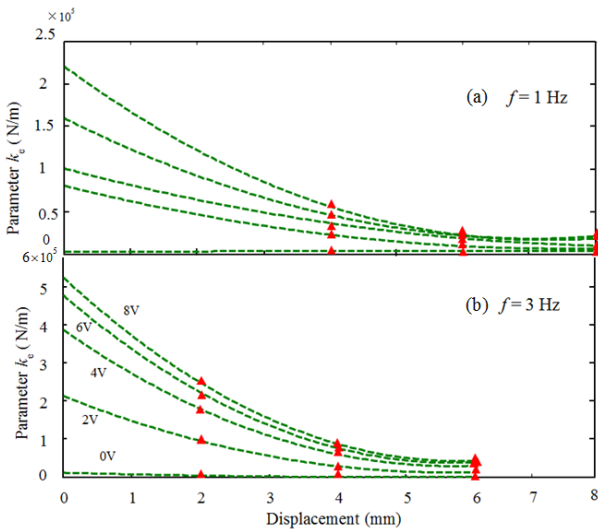


Fig. 9 Dependence of the stiffness coefficient k_e on the displacement amplitude A

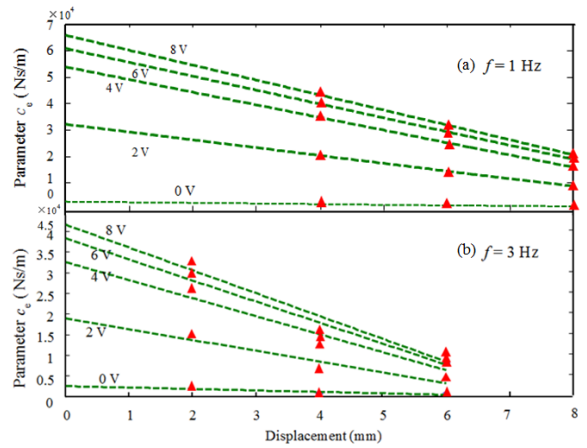


Fig. 12 Dependence of the viscous coefficient c_e on the displacement amplitude A

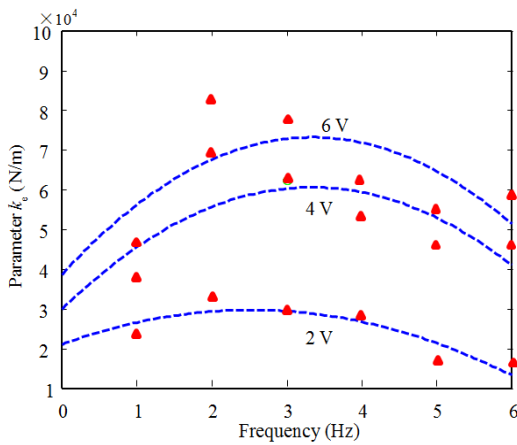


Fig. 10 Dependence of the stiffness coefficient k_e on the frequency f ($A = 4$ mm)

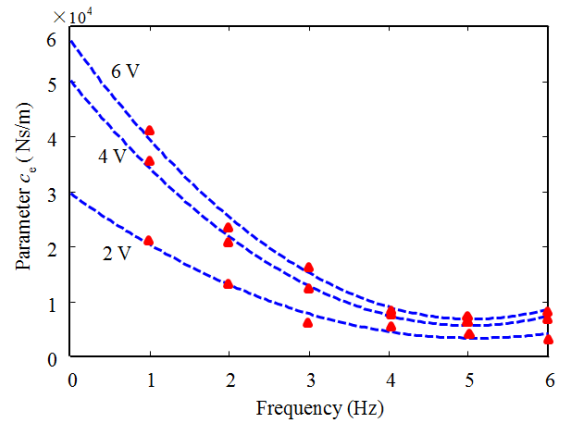


Fig. 13 Dependence of the viscous coefficient c_e on the frequency f ($A = 4$ mm)

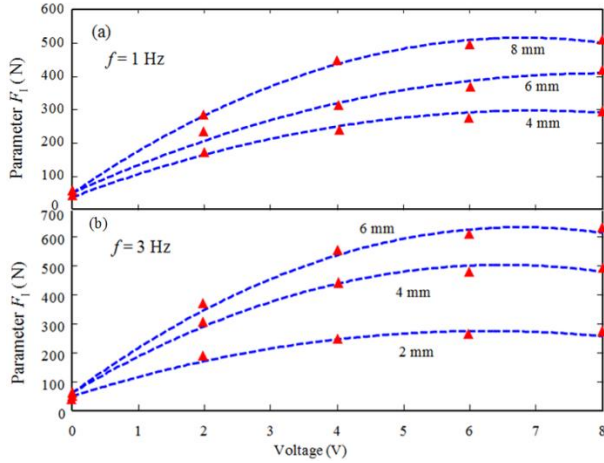


Fig. 14 Dependence of the frictional coefficient F_f on the voltage input V

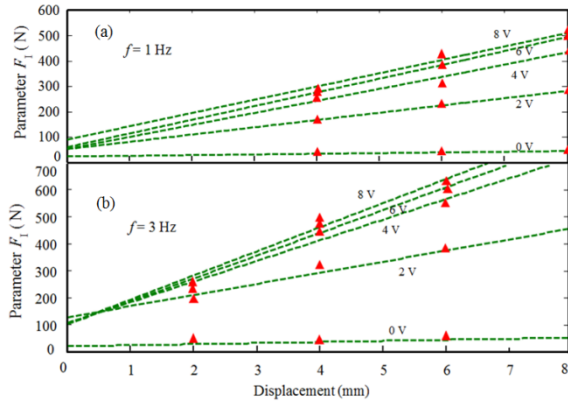


Fig. 15 Dependence of the frictional coefficient F_f on the displacement amplitude A

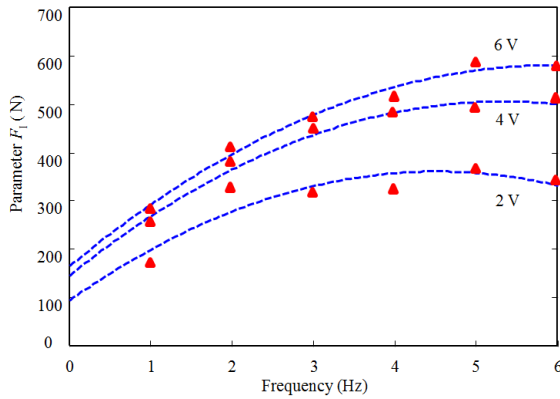


Fig. 16 Dependence of the frictional coefficient F_f on the frequency f ($A = 4$ mm)

In order to find out the variation in the parameters of the identified model of the MR damper, the tests on two randomly selected dampers of the same type were carried out. It was found that the parameters of different dampers were of slight difference, which indicated that the investigated type of MR damper is of good quality in stability.

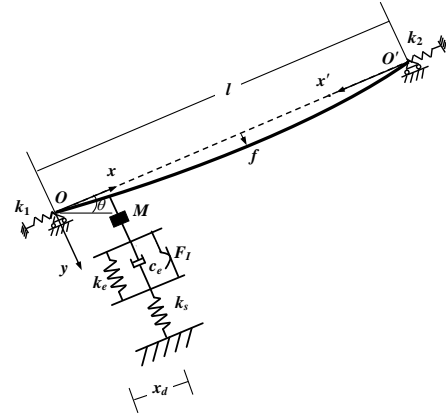


Fig. 17 Saged cable-damper system

4. Application in open-loop control of cable vibration

For a saged cable-damper system as shown in Fig. 17, the MR damper, represented by the concentrated damper mass M , stiffness coefficient k_e , viscous coefficient c_e , frictional coefficient F_f and support stiffness k_s , is located at the distance x_d from the lower end.

Supposing that the motion amplitude of the damper piston relative to its cover is A and the vibration frequency is f , for any given voltage input V to the MR damper, the damper parameters k_e , c_e , and F_f can be obtained by Eq. (3).

Using the equivalent energy method (Weber and Boston 2010, Huang and Jones 2011, Duan *et al.* 2019a, b), an equivalent damping coefficient c_l for frictional force F_f can be obtained

$$W = \int_0^T F_f \operatorname{sgn}(\dot{\Delta}) \cdot \dot{\Delta} dt = 4F_f \|\Delta\| \quad (4a)$$

$$W = \int_0^T c_l \dot{\Delta} \cdot \dot{\Delta} dt = c_l \pi \|\dot{\Delta}\| \|\Delta\| \quad (4b)$$

$$c_l = \frac{4F_f}{\pi \|\dot{\Delta}\|} \quad (4c)$$

For brevity, the following dimensionless parameters are defined

$$\eta_c = \frac{c_e}{\sqrt{T_0 m}} \quad (5a)$$

$$\eta_l = \frac{c_l}{\sqrt{T_0 m}} \quad (5b)$$

$$u_k = \frac{k_e l}{T_0} \quad (5c)$$

$$u_s = \frac{k_s l}{T_0} \quad (5d)$$

$$\gamma_M = \frac{M(\omega_n^0)^2 l}{T_0} \quad (5e)$$

where ω_n^0 , $n = 1, 2, 3, \dots$, is the circular frequency of the undamped cables.

The damping ratio ξ achieved by sagged cable-damper setup (Fig. 17) can then be determined from a general formula as (Duan *et al.* 2019b)

$$\frac{\xi_n}{l} = \frac{n\pi W_{\eta, \lambda^2} (\eta_c + \eta_l) \frac{x_d}{l}}{\left[1 + U_{k, m, s} + U_{k, m}\right]^2 + \left[n\pi W_{\eta, \lambda^2} (\eta_c + \eta_l) V_{m, s} \frac{x_d}{l}\right]^2} W_{\xi, \lambda^2} \quad (6a)$$

where

$$U_{k, m, s} = \frac{u_k}{u_s} (1 - \gamma_M \frac{x_d}{l}) \quad (6b)$$

$$U_{k, m} = (u_k - \gamma_M) \frac{x_d}{l} \quad (6c)$$

$$c_I = \frac{4F_l}{\pi \|\Delta\|} V_{m, s} = \left(\frac{1}{u_s} (1 - \gamma_M \frac{x_d}{l}) + \frac{x_d}{l} \right) \left/ \left(\frac{x_d}{l} \right) \right. \quad (6d)$$

The sag-extensibility parameter λ^2 (Irvine and Caughey 1974) can be obtained as 0.09 from Eq. (7)

$$\frac{1}{\lambda^2} = \left(\frac{L_e/l}{EA} + \frac{1}{k_1 l} + \frac{1}{k_2 l} \right) \frac{T_0^3}{(mgl \cos \theta)^2} \quad (7)$$

where m and T_0 are the mass per unit length and the cable tension force along the chord OO' (x -axis); l is the distance between the supports, and θ is the inclination angle (the angle between the chord OO' and the horizon); g is the gravity acceleration; EA is the axial elastic stiffness of the cable; k_1 and k_2 are the spring stiffness at the cable ends; L_e is the effective length as expressed in Eq. (8(a)) and can be approximated as l in practice; f is the sag at the mid span, as expressed in Eq. (8(b)).

$$L_e = \int_0^l \left(\frac{ds}{dx} \right)^3 dx \approx \left[1 + 8 \left(\frac{f}{l} \right)^2 \right] l \quad (8a)$$

$$f = \frac{mgl^2 \cos \theta}{8T_0} \quad (8b)$$

The modification factors W_{ξ, λ^2} and W_{η, λ^2} due to sage can be obtained by (Duan *et al.* 2009b)

$$W_{\xi, \lambda^2} = \begin{cases} 1 + 0.11\lambda^2(1 + 0.035\lambda^2)^2 & n = 1, \lambda^2 \leq 10 \\ 1 & n > 1, \lambda^2 \leq 10 \end{cases} \quad (9a)$$

Table 1 Main parameters of the studied cable

Parameter	EA (MN)	m (kg/m)	θ ($^\circ$)	T_0 (kN)	l (m)
Value	1254	51.8	36.9	3095	114.719

$$W_{\eta, \lambda^2} = \begin{cases} 1 + 0.035\lambda^2 & n = 1, \lambda^2 \leq 10 \\ 1 & n > 1, \lambda^2 \leq 10 \end{cases} \quad (9b)$$

The damping ratio ξ of the general cable-damper system can be obtained in an analytical way by Eq. (6), rather than by finite element model or time-consuming numerical simulation. The solution includes at least two aspects: (i) when the damper parameters are given, the achieved damping ratio for the cable-damper system can be obtained and therefore control strategies achieving maximum or sub-maximum damping ratios can be developed, which will be discussed later; (ii) when the parameters of the cable are given, a customized damper/support system that achieves the optimal or suboptimal control effectiveness can be designed.

In order to show the procedure in detail, we take one typical cable in a cable-stayed bridge as an example. The main parameters are shown in Table 1. The first three modal frequencies are 1.11 Hz, 2.23 Hz, and 3.34 Hz, respectively. Control strategies can be achieved by following steps.

(i) The sag-extensibility parameter λ^2 (Irvine and Caughey 1974) can be obtained as 0.09 from Eq. (7). According to Eq. (9), the modification factors W_{ξ, λ^2} and

W_{η, λ^2} can be taken as 1.

(ii) For any given voltage input V , vibration amplitude A , and modal frequency f , the damper stiffness k_e , damper coefficient c_e , frictional coefficient F_l , and their normalized counterparts u_k , η_c , η_l can be obtained from Eqs. (3)-(5) and . The support stiffness k_s , damper mass M , and their normalized counterparts u_s and γ_M can be determined according to the actual installation.

(iii) The achieved damping ratio is obtained by substituting the parameters into Eq. (6).

(iv) By changing the values for voltage input V , vibration amplitude A , and modal frequency f , the relationship among the achieved damping ratio ξ , voltage input V , vibration amplitude A , and modal frequency f is obtained.

5. Results and discussion

5.1 Optimal voltage input and its dependence on the vibration amplitude

Fig. 18 shows the normalized damping ratio of the third mode versus the voltage input V for various vibration amplitudes $A = 0.5$ mm, 2 mm, 4 mm, and 7 mm,

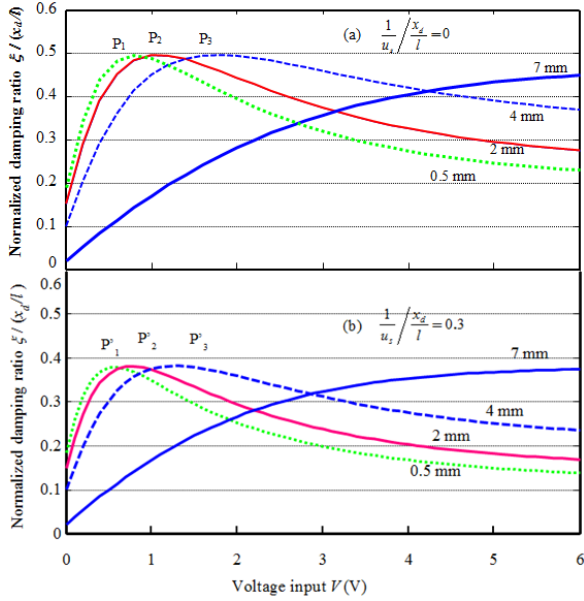


Fig. 18 Normalized damping ratio versus voltage input for various vibration amplitudes (3rd Mode, $\frac{x_d}{l} = 0.05$)

respectively, when the damper location $\frac{x_d}{l} = 0.05$. For amplitudes $A = 0.5$ mm, 2 mm, and 4 mm, it is observed that there is an optimal voltage for achieving the maximum damping ratio for each vibration amplitude, as indicated by P_1 , P_2 , P_3 in Fig. 18(a) or P'_1 , P'_2 , P'_3 in Fig. 18(b). It is obvious that the optimal voltage increases as the vibration amplitude increases. For $A = 7$ mm, the damping ratio increases as the voltage input increases and the optimal voltage does not appear. This is due to the limitations of the damping force provided by the selected MR damper. The damper force even when $V = 6$ V is not large enough to provide the maximum attainable damping ratio in this case.

5.2 Effect of damper support stiffness and damper stiffness on the maximum damping ratio and optimal voltage input

From the comparison of Figs. 18(a) and 18(b), it is observed that the support stiffness u_s plays an important role in decreasing both the maximum damping ratio and the optimal voltage (damper coefficient). For ideal support $\frac{1}{u_s} = 0$, the maximum normalized damping ratio is about 0.5 for each vibration amplitude; while for softened support $\frac{1}{u_s} \frac{x_d}{l} = 0.3$, the maximum normalized damping ratio decreases to 0.38, only about 75% of that for the ideal support. The optimal voltage correspondingly decreases from 0.8 V, 1.0 V, and 1.8 V to 0.6 V, 0.8 V, and 1.3 V, for the vibration amplitudes $A = 0.5$ mm, 2 mm, and 4 mm,

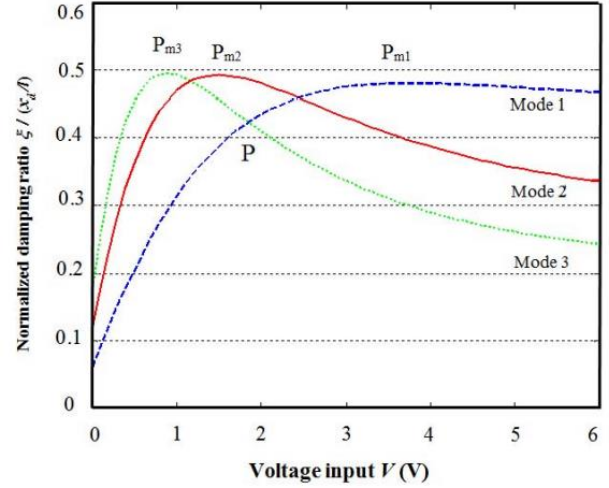


Fig. 19 Normalized damping ratio versus voltage input for different modes (Vibration amplitude $A = 1$ mm, $\frac{x_d}{l} = 0.05$)

respectively. It should be noted that the softening of the damping stiffness may result from the clearance of the connection between the damper and the support or between the damper and the cable, as well as from the flexibility of the support. Therefore, in actual installation, it is desirable to eliminate the connection clearance and use a sufficiently stiff support.

It is also seen that for the ideal support the maximum normalized damping ratio is almost the same, with the maximum attainable value of 0.5, at different vibration amplitudes. This indicates that for the present application the effect of the damper stiffness k_e or u_k is slight. It should be noted that the damper mass M or γ_M , which may increase the maximum damping ratio, is assumed to be zero.

5.3 Modal dependence of the optimal voltage input and design of multi-mode suboptimal open-loop control

For the linear viscous damper, the optimal damper coefficient achieving the maximum damping ratio is only dependent on the modal number but independent of the vibration amplitude; for the frictional damper, the optimal damper coefficient is only dependent on the vibration amplitude but independent of the vibration mode. However, for the used MR damper, which is a combined viscous and frictional damper, the optimal voltage achieving the maximum damping ratio is not only dependent on the vibration amplitude, but also dependent on the vibration mode. As shown in Fig. 19, the optimal voltage input is 3.8 V, 1.5 V, and 0.9 V, respectively, for the first three modes, when the vibration amplitude $A = 1$ mm and the damper location $\frac{x_d}{l} = 0.05$. It is obvious that the optimal voltage input is smaller for the higher vibration modes, similar to the case for the linear viscous damper (Pacheco *et al.* 1993).

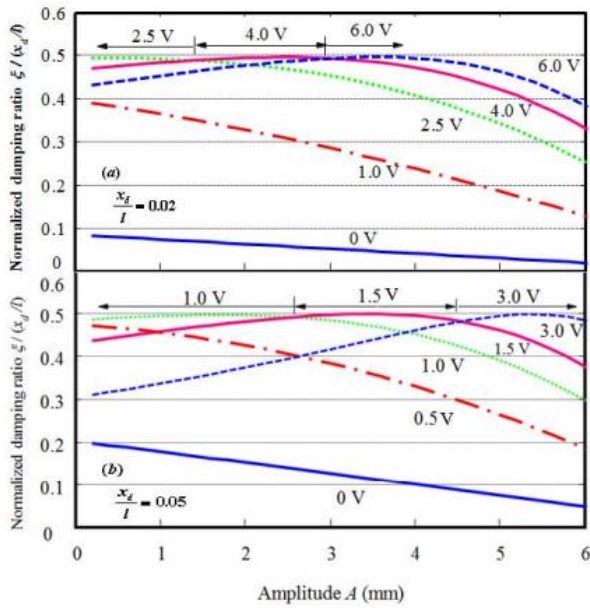


Fig. 20 Normalized damping ratio versus vibration amplitude for various voltage inputs (3rd Mode)

Fig. 19 also provides a design method for multi-mode suboptimal control. By setting the voltage input to 1.9 V, indicated by the intersection (P) of the curves for the first and third modes, a normalized damping ratio of no less than 0.42, indicated by the coordinate of P , can be achieved for all of the three modes (i.e., 0.42 for the first and third modes and 0.48 for the second mode).

5.4 Design of multi-switch single-mode optimal open-loop control

Since the optimal voltage input that achieves the maximum damping ratio changes with the vibration amplitude and vibration mode, the maximum or sub-maximum damping ratio can be achieved for different vibration amplitudes and any given vibration mode by tracking the optimal voltage input in a multi-switch way. For the third modal vibration as shown in Fig. 20 (a), when the damper location is $\frac{x_d}{l} = 0.02$, the optimal voltage is 2.5 V for amplitudes smaller than 1.5 mm, 4.0 V for amplitudes between 1.5 mm and 3.0 mm, and 6.0 V for amplitudes larger than 3.0 mm. By setting voltage inputs equal to 2.5 V, 4.0 V, and 6.0 V corresponding to these three ranges in amplitude, the maximum modal damping ratio can be always achieved. Fig. 20(a) also shows the normalized damping ratio achieved for voltage inputs of 0 V and 1 V.

The maximum attainable damping ratio ($\xi/\frac{x_d}{l} = 0.5$) cannot be achieved for any vibration amplitude range here, due to the excessively small damper force provided by these two voltage inputs. It should be noted that the case of 0 V gives the passive-off damping ratio by the MR damper, which can still be in function even when the power supply

fails. In contrast to Figs. 20(a) and 20(b) shows the case of $\frac{x_d}{l} = 0.05$, from which we see that the optimal voltage is 1.0 V for amplitudes of smaller than 2.4 mm, 1.5 V for amplitudes between 2.8 mm and 4.6 mm, and 3.0 V for amplitudes larger than 4.6 mm. Therefore, when the damper is located further away from the closer end of the cable (i.e., the value of $\frac{x_d}{l}$ is larger), the value of the optimal voltage input is smaller.

6. Conclusions

This paper presents the modelling of the full-scale MR damper RD-1005, based on experimental tests, and its application in the open-loop vibration control design of a 115 m long stay cable in single-damper setup. The results from those works are summarized as follows:

(i) A parameter-adaptive three-element model was developed for a full-scale MR damper and integrated into the general formula to evaluate the maximum attainable damping ratio of general cable-damper system.

(ii) There is an optimal voltage input that achieves the maximum modal damping ratio of the damper-cable system. It turns out that the softening of support stiffness due to the flexibility of the support and/or the clearance of the connections between the damper and the cable and between the damper and the support can obviously decrease the maximum damping ratio and the optimal voltage input. The damper stiffness of the damper RD-1005 is minor and its effect is not significant despite the fact that it decreases the maximum damping ratio and increases the optimal damper coefficient/voltage input. The optimal voltage input also depends on the vibration amplitude and vibration mode, as well as on the location of the damper. For a given vibration mode, the optimal voltage input increases as the vibration amplitude increases. For the same vibration amplitude, the optimal voltage is larger for the lower modes and smaller for the higher modes. For a given vibration amplitude and vibration mode, the optimal voltage input is larger when the damper is further away from the closer end of the cable. Therefore, after the location of the damper has been decided, the multi-mode suboptimal open-loop control and multi-switch single-mode optimal open-loop control strategies can be applied to achieve the sub-maximum or maximum damping ratio for different vibration amplitudes and different vibration modes.

Acknowledgments

This research work was supported by the National Natural Science Foundation of China (U1709216, 51608478, 51522811, 51478429, and 90915008), the National Key R&D Program of China (2017YFC0806100), the grant from the Ministry of Science and Technology of China (2018YFE0190100), the grant from the Research Grants Council of the Hong Kong Special Administrative Region, China (Project No. PolyU 5252/07E), and the grant

from The Hong Kong Polytechnic University through the Development of Niche Areas Programme (Project No. 1-BB95).

References

- Butz, T. and Stryk, O.V. (2002), "Modelling and simulation of electro- and magnetorheological fluid dampers", *ZAMM-Zeitschrift für Angewandte Mathematik und Mechanik*, **82**(1), 3-20. [https://doi.org/10.1002/1521-4001\(200201\)82:1<3::AID-ZAMM3>3.0.CO;2-O](https://doi.org/10.1002/1521-4001(200201)82:1<3::AID-ZAMM3>3.0.CO;2-O).
- Carlson, J.D. and Spencer, B.F., Jr. (1996), "Magneto-rheological fluid dampers for semi-active seismic control", *Proceedings of the 3rd International Conference on Motion and Vibration Control*, Chiba, Japan, September.
- Chen, Z.Q., Wang, X.Y., Ko, J.M., Ni, Y.Q., Spencer, B.F., Jr., Yang, G. and Hu, J.H. (2004), "MR damping system for mitigating wind-rain induced vibration on Dongting Lake Cable-Stayed Bridge", *Wind Struct.*, **7**(5), 293-304. <http://dx.doi.org/10.12989/was.2004.7.5.293>.
- Duan, Y.F. (2004), *Vibration Control of Stay Cables Using Semi-active Magneto-rheological (MR) Dampers*, Ph.D. Dissertation, The Hong Kong Polytechnic University, Hong Kong.
- Duan, Y.F., Ni, Y.Q. and Ko, J.M. (2005), "State - derivative feedback control of cable vibration using semiactive magnetorheological dampers", *Comput. - Aided Civil Infrastruct. Eng.*, **20**(6), 431-449. <https://doi.org/10.1111/j.1467-8667.2005.00396.x>.
- Duan, Y.F., Ni, Y.Q. and Ko, J.M. (2006), "Cable vibration control using Magneto-rheological (MR) dampers", *J. Intel. Mat. Syst. Str.*, **17**(4), 321-325. https://doi.org/10.1142/9789812702197_0121.
- Duan, Y.F., Ni, Y.Q., Zhang, H.M., Spencer, B.F., Jr. and Ko, J.M. (2019a), "Design formulas for vibration control of taut cables using passive MR dampers", *Smart Struct. Syst.*, Accepted.
- Duan, Y.F., Ni, Y.Q., Zhang, H.M., Spencer, B.F., Jr. and Ko, J.M. (2019b), "Design formulas for vibration control of sagged cables using passive MR dampers", *Smart Struct. Syst.*, Accepted.
- Guan, X.C., Huang Y., Li, H. and Ou, J.P. (2012), "Adaptive MR damper cable control system based on piezoelectric power harvesting", *Smart Struct. Syst.*, **10**(1), 33-46. <http://dx.doi.org/10.12989/sss.2012.10.1.033>.
- Hikami, Y. and Shiraishi, N. (1988), "Rain-wind induced vibrations of cables in cable stayed bridges", *J. Wind Eng. Ind. Aerod.*, **29**, 409-418.
- Huang, H.W., Liu, J.Y. and Sun, L.M. (2015), "Full-scale experimental verification on the vibration control of stay cable using optimally tuned MR damper", *Smart Struct. Syst.*, **16**(6), 1003-1021. <http://dx.doi.org/10.12989/sss.2015.16.6.1003>.
- Huang, Z.H. and Jones N.P. (2011), "Damping of taut-cable systems: effects of linear elastic spring support", *J. Eng. Mech.*, **137**(7), 512-518. [https://doi.org/10.1061/\(ASCE\)EM.1943-7889.0000252](https://doi.org/10.1061/(ASCE)EM.1943-7889.0000252).
- Irvine, H.M., and Caughey, T.K. (1974), "The linear theory of free vibrations of a suspended cable", *Proceedings of the Royal Society A: Mathematical, Physical and Engineering Sciences*, **341**(1626), 299-315. <https://doi.org/10.1098/rspa.1974.0189>.
- Jing, H.Q., Xia, Y., Xu, Y.L. and Li, Y.L. (2016), "Measurement of rivulet movement and thickness on inclined cable using videogrammetry", *Smart Struct. Syst.*, **18**(3), 485-500. <https://doi.org/10.12989/sss.2016.18.3.485>.
- Johnson, E.A., Baker, G.A., Spencer, B.F., Jr. and Fujino, Y. (2007), "Semiactive damping of stay cables", *J. Eng. Mech. - ASCE*, **133**(1), 1-11. [https://doi.org/10.1061/\(ASCE\)0733-9399\(2007\)133:1\(1\)](https://doi.org/10.1061/(ASCE)0733-9399(2007)133:1(1)).
- Jung, H.J., Spencer, Jr. B.F., Ni, Y.Q. and Lee, I.W. (2004), "State-of-the-art of semiactive control systems using MR fluid dampers in civil engineering applications", *Struct. Eng. Mech.*, **17**(3), 493-526. http://dx.doi.org/10.12989/sem.2004.17.3_4.493.
- Kazakov, Y. B., Morozov, N. A. and Nesterov, S.A. (2016), "Development of models of the magnetorheological fluid damper", *J. Magn. Magn. Mater.*, **431**, 269-272. <https://doi.org/10.1016/j.jmmm.2016.10.006>.
- Ko, J.M., Ni, Y.Q., Chen, Z.Q. and Spencer, Jr. B.F. (2002), "Implementation of MR dampers to Dongting Lake Bridge for cable vibration mitigation", (Ed., Casciati, F.), *Proceedings of the 3rd World Conference on Structural Control*, Como, Italy, April.
- Ko, J.M., Zheng, G., Chen, Z.Q. and Ni, Y.Q. (2002). "Field vibration tests of bridge stay cables incorporated with magnetorheological (MR) dampers", *Smart Structures and Materials 2002: Smart Systems for Bridges, Structures, and Highways*, (Eds., S.C. Liu and D.J. Pines), SPIE 4696, 30-40.
- Li, H., Liu, M., Li, J.H., Guan, X.C. and Ou, J.P. (2007), "Vibration control of stay cables of the Shandong Binzhou Yellow River Highway Bridge using magnetorheological fluid dampers", *J. Bridge Eng.*, **12**(4), 401-409. [https://doi.org/10.1061/\(ASCE\)1084-0702\(2007\)12:4\(401\)](https://doi.org/10.1061/(ASCE)1084-0702(2007)12:4(401)).
- Matsumoto, M., Saitoh, T., Kitazawa, M., Shirato, H. and Nishizaki, T. (1995), "Response characteristics of rain-wind induced vibration of stay-cables of cable-stayed bridges", *J. Wind Eng. Ind. Aerod.*, **57**(2-3), 323-333. [https://doi.org/10.1016/0167-6105\(95\)00010-O](https://doi.org/10.1016/0167-6105(95)00010-O).
- Ni, Y.Q., Wang, X.Y., Chen, Z.Q. and Ko, J.M. (2007), "Field observations of rain-wind-induced cable vibration in cable-stayed Dongting Lake Bridge", *J. Wind Eng. Ind. Aerod.*, **95**(5), 303-328. <https://doi.org/10.1016/j.jweia.2006.07.001>.
- Pacheco, B.M., Fujino, Y. and Sulekh, A. (1993), "Estimation curve for modal damping in stay cables with viscous damper", *J. Struct. Eng. - ASCE*, **119**(6), 1961-1979. [https://doi.org/10.1061/\(ASCE\)0733-9445\(1993\)119:6\(1961\)](https://doi.org/10.1061/(ASCE)0733-9445(1993)119:6(1961)).
- Persoon, A.J. and Noorlander, K. (1999), "Full-scale measurements on the Erasmus Bridge after rain/wind induced cable vibrations", (Eds., Larsen, A., Larose, G.L. and Livesey, F.M.), *Wind Engineering into the 21st Century*. Rotterdam: Balkema, the Netherlands, June.
- Poston, R.W. (1998), "Cable-stay conundrum", *ASCE Civil Eng.*, **68**(8), 58-61.
- Powell, J.A. (1994), "Modeling the oscillatory response of an electrorheological fluid", *Smart Mater. Struct.*, **3**(4), 416-438.
- Sun, L.M., Hong, D.X. and Chen, L. (2017), "Cables interconnected with tuned inerter damper for vibration mitigation", *Eng. Struct.*, **151**, 57-67. <https://doi.org/10.1016/j.engstruct.2017.08.009>.
- Tanaka, H. (2003), "Aerodynamics of cables", In: *Proceedings of the 5th International Symposium on Cable Dynamics*, Santa Margherita Ligure, Italy, September.
- Verwiebe, C. (1998), "Rain-wind-induced vibrations of cables and bars", (Eds., Larsen, A. and Esdahl, S.), *Bridge Aerodynamics: Proceedings of the International Symposium on Advances in Bridge Aerodynamics*. Copenhagen, Denmark, May.
- Virlogeux, M. (1998), "Cable vibrations in cable-stayed bridges", (Eds., Larsen A. and Esdahl S.), *Bridge aerodynamics: Proceedings of the International Symposium on Advances in Bridge Aerodynamics*, Copenhagen, Denmark, May.
- Wang, X.Y., Ni, Y.Q., Ko, J.M. and Chen, Z.Q. (2005), "Optimal design of viscous dampers for multi-mode vibration control of bridge cables", *Eng. Struct.*, **27**(5), 792-800.
- Wang, Z.H., Chen, Z.H., Gao, H. and Wang, H. (2018), "Development of a self-powered magnetorheological damper

- system for cable vibration control”, *Appl. Sci. Basel*, **8**(1), 118. <https://doi.org/10.3390/app8010118>.
- Wang, W., Hua, X. and Wang X. (2019), “Mechanical behavior of magnetorheological dampers after long-term operation in a cable vibration control system”, *Struct. Control Health Monit.*, **26**(1), e2280. <https://doi.org/10.1002/stc.2280>.
- Weber, F. and Boston, C. (2010), “Energy based optimization of viscous-friction dampers on cables”, *Smart Mater. Struct.*, **19**(4), 045025.
- Zhou, H.J., Huang X.J., Xiang N., He J.W., Sun, L.M. and Xing, F. (2018), “Free vibration of a taut cable with a damper and a concentrated mass”, *Struct. Control Health Monit.*, **25**(11), 1-21. <https://doi.org/10.1002/stc.2251>.
- Zhou, H.J., Xiang, N. and Huang, X. (2018), “Full-scale test of dampers for stay cable vibration mitigation and improvement measures”, *Struct. Monit. Maint.*, **5**(4), 489-506. <https://doi.org/10.12989/smm.2018.5.4.489>.
- Zhou, H.J. and Sun, L.M. (2013), “Damping of stay cable with passive-on magnetorheological dampers: a full-scale test”, *Int. J. Civil Eng.*, **11**(3), 154-159.
- Zhou, H.J., Sun, L.M. and Xing, F. (2014), “Damping of full-scale stay cable with viscous damper: experiment and analysis”, *Adv. Struct. Eng.*, **17**(2), 265-274. <https://doi.org/10.1260/1369-4332.17.2.265>.